



Early and Delayed Alteration of Atrial Electrograms Around Single Radiofrequency Ablation Lesion

Stepan Havranek^{1*}, Hana Alfredova¹, Zdenka Fingrova¹, Lucie Souckova¹ and Dan Wichterle^{1,2}

¹ Second Department of Medicine—Department of Cardiovascular Medicine, First Faculty of Medicine, Charles University and General University Hospital in Prague, Prague, Czechia, ² Department of Cardiology, Institute for Clinical and Experimental Medicine, Prague, Czechia

OPEN ACCESS

Edited by:

Shimon Rosenheck,
Meir Medical Center, Israel

Reviewed by:

Jacqueline Joza,
McGill University Health Centre,
Canada

Antonio Sorgente,
Cleveland Clinic Abu Dhabi,
United Arab Emirates

Benjamin Berte,
Hirslanden Klinik Im Park, Switzerland

*Correspondence:

Stepan Havranek
stepan.havranek@lf1.cuni.cz

Specialty section:

This article was submitted to
Cardiac Rhythmology,
a section of the journal
Frontiers in Cardiovascular Medicine

Received: 10 September 2018

Accepted: 17 December 2018

Published: 08 January 2019

Citation:

Havranek S, Alfredova H, Fingrova Z,
Souckova L and Wichterle D (2019)
Early and Delayed Alteration of Atrial
Electrograms Around Single
Radiofrequency Ablation Lesion.
Front. Cardiovasc. Med. 5:190.
doi: 10.3389/fcvm.2018.00190

Purpose: The acute effect of radiofrequency (RF) ablation includes local necrosis and oedema. We investigated the spatiotemporal change of atrial electrograms in the area surrounding the site of single standardized pulse of RF energy.

Methods: The study enrolled 12 patients (45–67 years, 10 males) with paroxysmal atrial fibrillation (AF) undergoing ablation procedure with irrigated-tip ablation catheter and 3D navigation. The high-density mapping/remapping (129 ± 63 points) within the circular area with radius of ~ 10 mm, centered at the pre-specified posterior left pulmonary vein antrum ablation site was performed at baseline, immediately after single RF energy delivery (25 W, 30 s, 20 ml/min) and after 30 min waiting period. Bipolar voltages of atrial electrograms (A-EGM-biV) were averaged within the central and 12 adjacent left atrium segments and their relative change was studied.

Results: After the ablation, overall A-EGM-biV within the mapping zone (3.51 ± 1.89 mV at baseline) reduced to 2.83 ± 1.77 mV (immediately) and to 2.68 ± 1.58 mV (after 30 min waiting period). In per-segment pair-wise comparison, we observed highly significant change in A-EGM-biV that extended up to the distance of 8.8 mm from the lesion core. The maximum early A-EGM-biV attenuation by 39–49% ($P < 0.001$) was registered in segments adjacent to pulmonary vein ostia. The subsequent (delayed) A-EGM-biV reduction by 17–24% ($P < 0.05$) was observed in opposite direction from the lesion center.

Conclusions: Significant alteration of atrial electrograms was detectable rather distant from the central lesion. Spatiotemporal development of ablation lesion was eccentric/asymmetric. While acute A-EGM-biV reduction can be attributed predominantly to direct thermal injury, delayed effects are probably due to oedema progression.

Keywords: radiofrequency catheter ablation, atrial fibrillation, pulmonary vein isolation, electrogram voltage, oedema

INTRODUCTION

Pulmonary vein (PV) isolation (PVI) for atrial fibrillation (AF) is an established therapy in selected patients (1). Nevertheless, resumption of PV-left atrial (LA) conduction is exceedingly common and thought to be responsible for the vast majority of post-ablation atrial tachyarrhythmia recurrences (2).

It is well-known, that the acute effect of radiofrequency (RF) ablation consists of local necrosis, collateral oedema, and atrial stunning (3, 4). In the absence of cellular death, reversible tissue oedema or thermal stunning may account for the discordance between the incidence of acute and chronic PVI (5–7), because injured, but still viable, myocardium may eventually recover its conduction properties and result in late PV reconnection (8). Furthermore, the phenomenon of oedema may protect the ablative energy from reaching the deeper layers of the myocardium and could be one of the reasons for the difficulty in creating conduction block.

Inspection of atrial electrogram (A-EGM) morphological/voltage change during ablation is well-recognized method for the assessment of lesion efficacy. However, conduction gaps are frequently located in epicardial layers of atrial myocardium. The larger distance from endocardially-positioned catheter bipole may be also augmented by the oedema-induced thickening of the atrial wall. Therefore, gap-related electrical activities might be difficult to identify because of far-field morphology of corresponding A-EGMs (9).

Understanding the factors that influence A-EGM voltages might improve ablation effectiveness and clinical outcome. However, data on the immediate effect of RF lesion on A-EGM voltages are lacking. The aim of this prospective study was to investigate the spatiotemporal change of A-EGM in the area surrounding the site of single standardized pulse of RF energy.

METHODS

The study was approved by the local ethics committee and all patients signed an informed consent with the procedure. All antiarrhythmic drugs except amiodarone were discontinued for at least five half-lives prior to the study. Consecutive patients undergoing PVI for paroxysmal AF without structural heart disease who had no low voltage areas identified at the posterior LA wall (bipolar voltage <0.5 mV) during point-by-point electroanatomic mapping and who were in sinus rhythm at the beginning of the study protocol were enrolled.

Ablation Procedure

The catheter ablation was performed in fasting state under the mild analgosedation with midazolam and fentanyl. It was guided by electroanatomic mapping using a CARTO™ system (Biosense-Webster, Diamond Bar, CA, USA) and intracardiac echocardiography (AcuNav™ catheter, Siemens, Germany) according to local standards. Briefly, after double transseptal puncture, the single 20-polar circular catheter (Lasso™, Biosense-Webster, Diamond Bar, CA, USA) were placed at the ostia of PVs to record PV potentials. An LA reconstruction was achieved by point-by-point electroanatomic

mapping with an open irrigation 3.5-mm-tip ablation catheter (NaviStar Thermocool, Biosense-Webster) during sinus rhythm. Tagging of PV ostia on the electroanatomic map was facilitated by intracardiac echocardiography. Radiofrequency (RF) energy was delivered (EP Shuttle™, Stockert, Freiburg, Germany) for 30 s in the power-control mode (20–30 W) with irrigation flow rate of 20 ml/min (Cool Flow™ pump, Biosense-Webster) and the temperature limit of $<42^{\circ}\text{C}$. The energy was reduced when ablated in posterior antrum of PVs. Intravenous heparin was administered to maintain an activated clotting time of >300 s throughout the procedure. Single circumferential set of RF lesions was used to isolate ipsilateral PVs. The end-point of the PVI was defined as the disappearance or dissociation of PV potentials as well as the loss of capture of the LA by circumferential pacing from all PVs.

Study Protocol

Patients without stable sinus rhythm were excluded. After completing the electroanatomic map of LA, the optimum site for “study” ablation was found and tagged at the smooth posterior LA wall at the intended wide circumferential isolation line. The catheter stability with minimum sliding was verified by intracardiac echocardiography and stable A-EGM morphology. The site of “study” ablation was also selected to allow comfortable catheter navigation and mapping in its neighborhood in order to prevent mechanical irritation with excessive production of atrial premature complexes. High-density voltage remapping within the circular area with radius of ~ 10 mm, centered at the tagged point was performed (Map 1). Single pulse of RF energy (25 W/30 s/irrigation of 20 ml/min) was delivered to the pre-specified target site under the control of catheter stability as described above (Figure 1A). The high-density remapping within the same area was performed immediately after the RF energy delivery (Map 2) and repeated after 30 min waiting period (Map 3). During this period the right-sided PV were isolated. Finally, isolation of left-sided PVs was finished.

Data Processing

All three high-density remaps were meticulously inspected and manually edited to exclude all artifacts and cardiac cycles of non-sinus origin. Three-dimensional coordinates and corresponding bipolar voltages (A-EGM-biV) at all remapping points were exported and processed by purpose-written software. Specifically, points were projected to optimum common “en face” plane with ablation spot in the center. They were subsequently assigned to the central or one of 12 adjacent LA segments and their A-EGM-biV were averaged for each segment. The central segment had radius of 3 mm (area 28.3 squared mm). The external radii of adjacent segments were set to 6.7 and 10.8 mm for middle and outer segments, respectively, to get identical area for all segments (Figure 1B). Consequently, the mean distances of middle and outer segments from the lesion core was 4.9 and 8.8 mm, respectively.

Statistical Analysis

Continuous variables were expressed as means with standard deviations and compared by the two-tailed *t*-test for dependent

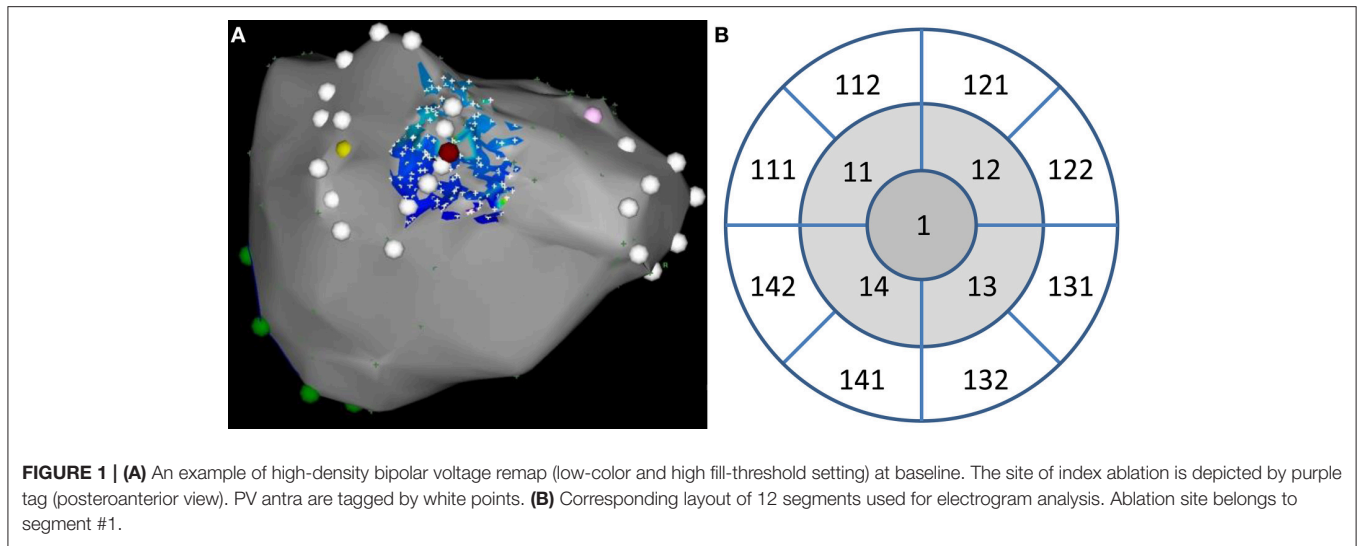


TABLE 1 | Baseline demographical, clinical, and procedure characteristics.

N	12
Males	10 (83%)
Age (years)	61 (45–67)
Arterial hypertension	8 (67%)
Diabetes mellitus	1 (8.3%)
Coronary artery disease	1 (8.3%)
Indexed LA volume estimated by ECHO (ml/m ²)	36 (32–36)
Left ventricular ejection fraction (%)	61 (62–65)
LA volume estimated by 3D electro-anatomical mapping (ml)	118 (102–144)
Amiodarone	1 (8.3%)
Mapping points—dense map # 1	113 (54–167)
Mapping points—dense map # 2	114 (69–160)
Mapping points—dense map # 3	151 (110–191)

Values are in format median (interquartile range) or n (%). LA, left atrium.

or independent samples, as appropriate. Not normally distributed variables were expressed as medians and interquartile range (IQR) and compared by Mann-Whitney *U*-test or Wilcoxon matched-pairs test, as appropriate. A *P* < 0.05 was considered significant. All analyses were performed using STATISTICA version 12 software (Statsoft, Inc., Tulsa, USA).

RESULTS

Out of 17 enrolled patients, two patients were excluded because of presence of low-voltage areas at the posterior LA wall and three patients were excluded because of AF onset during the study protocol. A total of 12 patients (10 males) with median age of 61 (IQR: 54–67) years were finally analyzed. Their baseline clinical and procedural characteristics are shown in **Table 1**.

Overall (mean of per-segment means) A-EGM-biV was 2.39 ± 1.34 mV at baseline. A-EGM-biV in individual segments at

TABLE 2 | Absolute values of bipolar atrial electrogram voltages in individual segments at baseline and two remapping periods.

	Map 1 (baseline)	Map 2 (after 5 min)	Map 3 (after 30 min)
1	2.33 ± 1.09	1.36 ± 0.66	1.08 ± 0.57
11	1.99 ± 1.12	0.87 ± 0.40	0.93 ± 0.46
12	2.79 ± 1.13	2.10 ± 1.19	1.74 ± 0.91
13	3.14 ± 1.46	2.49 ± 1.13	2.02 ± 1.00
14	1.95 ± 0.85	1.04 ± 0.46	0.91 ± 0.50
111	1.34 ± 0.89	0.91 ± 0.66	0.90 ± 0.73
112	1.83 ± 1.01	1.18 ± 0.78	1.30 ± 0.90
121	2.29 ± 1.46	1.95 ± 1.02	2.20 ± 0.80
122	3.50 ± 1.75	3.17 ± 1.57	2.94 ± 1.56
131	3.26 ± 1.61	3.77 ± 1.53	3.04 ± 1.58
132	3.01 ± 1.26	3.06 ± 1.31	2.36 ± 1.10
141	2.15 ± 0.91	1.50 ± 0.79	1.35 ± 0.69
142	1.60 ± 0.94	0.92 ± 0.51	0.92 ± 0.54

Values are in format mean ± SD. Localization of segment: see **Figure 1**. Map 1: baseline, Map 2: <5 min after index ablation, Map 3: >30 min after index ablation.

baseline, immediately after ablation and after 30 min are depicted in **Table 2**. Overall A-EGM-biV was significantly lower (1.76 ± 1.05 mV, *p* < 0.0001) in segments adjacent to PV ostia (# 11, 111, 112, 14, 141, and 142) compared to outer segments (2.69 ± 1.49 mV).

Representative example of A-EGM change exactly at the site of ablation is shown in **Figure 2**. In the whole mapping zone, we observed significant reduction in overall A-EGM-biV from 2.39 ± 1.34 mV to 1.84 ± 1.34 mV immediately after ablation and 1.66 ± 1.17 mV after 30 min waiting period (both *P* < 0.01).

Table 3 shows per-segment pair-wise comparison of relative changes of A-EGM-biV between all three high-density maps. With central segment excluded, the maximum early A-EGM-biV attenuation (Map 2–Map 1) up to –49% (*P* < 0.001) was observed in segments adjacent to pulmonary vein ostia (**Figure 3**). The delayed A-EGM-biV reduction (Map 3–Map 2)

up to -24% ($p < 0.05$) was most prominent in opposite direction from the lesion center (Figure 4).

DISCUSSION

The major finding of the study is that spatiotemporal development of single ablation lesion in PV antrum was eccentric/asymmetric with prominent initial A-EGM voltage reduction in regions adjacent to PV ostia and delayed A-EGM voltage decrease expanded in opposite direction. With respect to time-specific changes of ablation lesion, we hypothesize that detected delayed bipolar A-EGM voltages reduction, especially at regions adjacent to posterior wall and inferior segments, is due to tissue swelling.

It is well known that RF energy causes resistive heating of the tissue in the proximity of ablation catheter tip, followed by conductive heating of surrounding tissue (3). As the radial distribution of tissue temperature follows an inverse proportion with increasing distance from the catheter tip, an area with sublethal temperature surrounds the zone of permanent damage (3). The pathological studies have shown that acute lesion created by RF current consists of a central zone of coagulation necrosis surrounded by a zone of hemorrhage and inflammation followed by oedema (10–14). The existence of surrounding oedema after ablation was confirmed in different imaging studies based on

echocardiography (13, 15–22), cardiac MRI (14, 23–25), electron beam tomography (22) or ultrasound-based shear elastography (26). Pre-clinical pathologic and ultrasound data suggest that RF ablation-mediated cardiomyocyte and interstitial oedema occur almost immediately after energy delivery, and extends beyond the point of ablation (13). In another echocardiographical case series, the early appearance (within 15 s) of oedema during energy delivery was observed (17). In MRI study, Lardo et al. detected that lesions reached maximum size 5 min after ablation, whereas lesion signal intensity increased linearly with time but then reached a plateau at 12 min, which seems to be consistent with the temporal physiology of local acute interstitial oedema (14). Ultrasound-based elastography imaging techniques detected an immediate increase in tissue stiffness during RF delivery. The relative stiffness in the region adjacent to the area of stiffness increased slightly during the first 15 min, consistent with local fluid displacement (26).

In the context of lesion physiology, an acute A-EGM-biV reduction immediately after ablation in central zone close to ablation core corresponds most likely to direct thermal injury. However, since immediate oedema formation during RF delivery was observed in the real-time ultrasound study (27), its participation in early attenuation of A-EGM cannot be ruled out. Interestingly, the voltage reduction after ablation has asymmetrical distribution with larger voltage reduction in segments adjacent to PV ostia. We propose three possible explanations of this phenomena. First, the myocardium sleeves covering the PVs become gradually thinner toward the pulmonary segment of the vein and ended distinctly (28). Relatively deeper energy penetration may be expected in thinner myocardium in the direction to PV ostia, despite increasing distance from the ablation electrode. Second, single ablation in PV antrum leads to loss of direct electrical continuity resulting in change of direction of impulse propagation in the segments between the RF lesion and PV ostia. Consequently, propagation of the waveform that is more perpendicular to the mapping

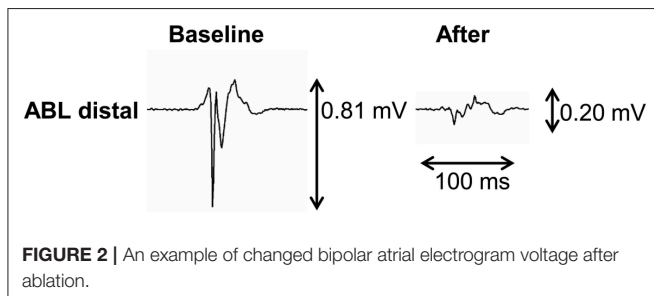
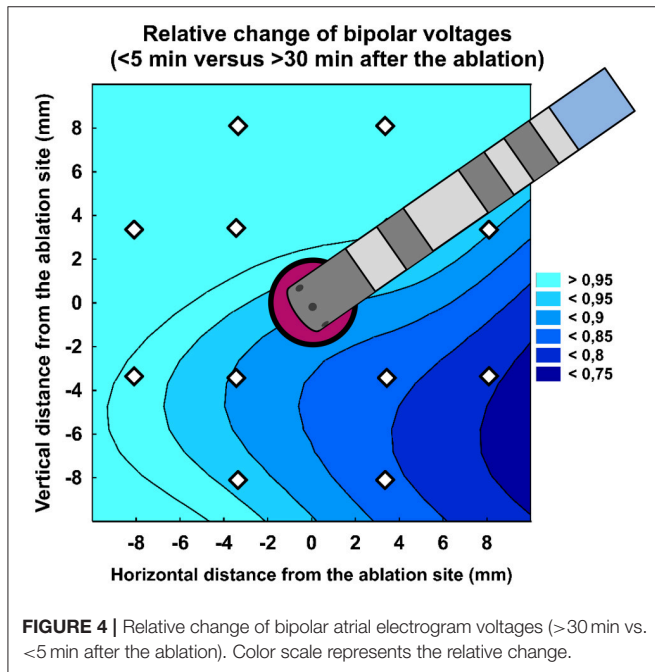
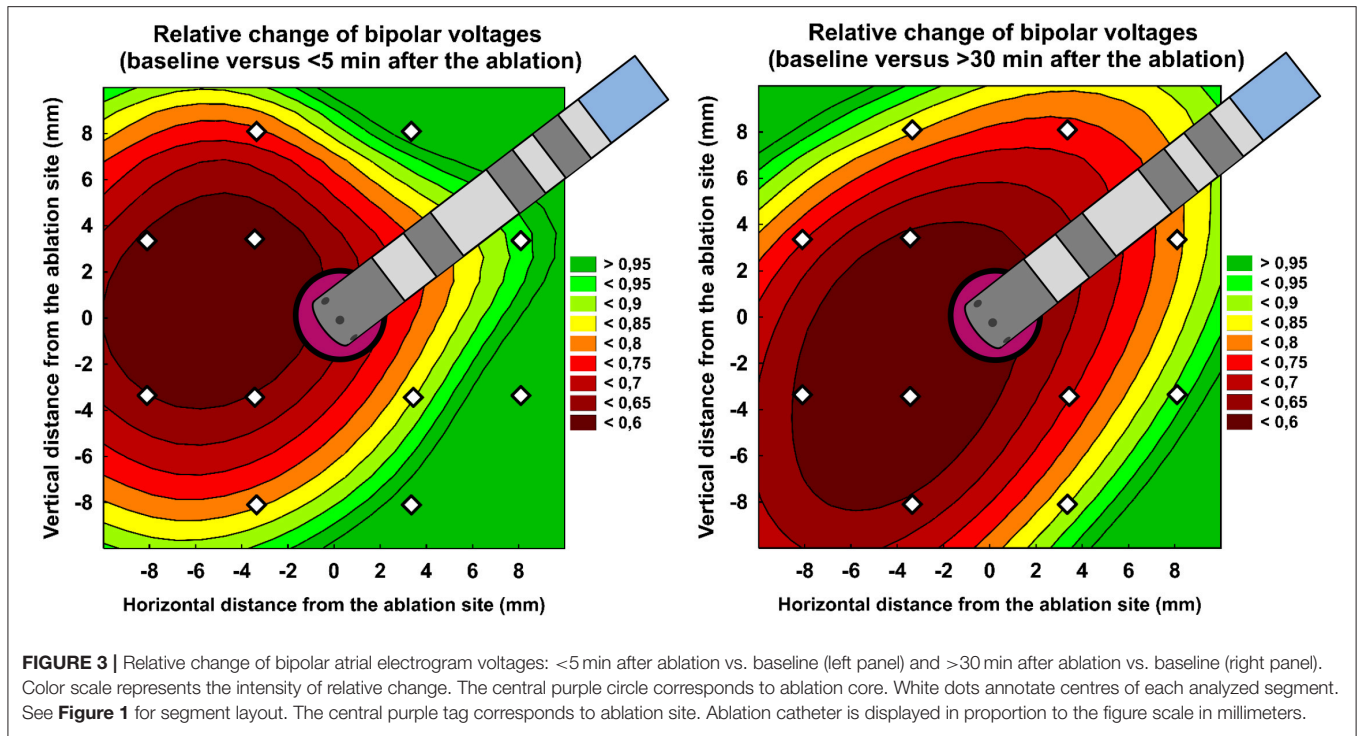


TABLE 3 | Relative change in bipolar atrial electrogram voltages in individual segments between consecutive maps.

Segment	Map 2/1	p^1	Map 3/1	p^2	Map 3/2	p^3
1	0.66 ± 0.24	0.0008	0.60 ± 0.38	0.006	0.86 ± 0.35	0.21
11	0.51 ± 0.26	0.0003	0.54 ± 0.23	0.0002	1.09 ± 0.26	0.25
12	0.71 ± 0.27	0.005	0.64 ± 0.26	0.001	1.10 ± 1.04	0.75
13	0.84 ± 0.36	0.16	0.70 ± 0.33	0.009	0.83 ± 0.18	0.007
14	0.62 ± 0.28	0.001	0.52 ± 0.24	0.00005	0.87 ± 0.33	0.21
111	0.60 ± 0.20	0.0001	0.70 ± 0.39	0.04	1.19 ± 0.69	0.39
112	0.71 ± 0.23	0.003	0.83 ± 0.32	0.12	1.32 ± 0.67	0.15
121	1.12 ± 1.05	0.77	0.73 ± 0.29	0.047	1.13 ± 0.36	0.35
122	0.86 ± 0.20	0.07	0.79 ± 0.19	0.01	0.90 ± 0.15	0.06
131	1.24 ± 0.32	0.045	0.92 ± 0.39	0.49	0.76 ± 0.27	0.01
132	1.05 ± 0.23	0.46	0.85 ± 0.31	0.13	0.81 ± 0.25	0.03
141	0.78 ± 0.59	0.25	0.61 ± 0.22	0.0001	0.95 ± 0.33	0.58
142	0.61 ± 0.27	0.0007	0.60 ± 0.25	0.0002	0.98 ± 0.34	0.84

Values are in format mean ± SD. p^1 —comparison of Map 2 and 1; p^2 —Map 3 and 1; p^3 —Map 3 and 2, respectively. Localization of segment: see Figure 1. Map 1: baseline, Map 2: <5 min after index ablation, Map 3: >30 min after index ablation.



catheter bipole can be associated with A-EGM-biV reduction. Third, the geometrical center of recorded A-EGM is in the middle between centers of two distal electrodes of mapping catheter, i.e., ~3 mm from the catheter tip and might not precisely match the sensor position. When catheter is positioned parallel to atrial wall during mapping of posterior left PV antra, such a mismatch may

be responsible for biased projection of local electrograms relative to the anatomical tag of ablation site.

The finding of temporal and spatial A-EGM-biV reduction is not a fully novel observation. It is well known, that PVI leads to the injury of myocardial tissue adjacent to antrum, which may contribute to the reduction of atrial voltage after PVI. The absence of voltage reduction in the atrial wall 1 cm from the PV lesions at the end of PVI was related to recurrent AF (29). It has also been observed, that the oedematous changes in the LA wall often extended to regions remote from the PVs, where the RF ablation was not applied. Duytschaever et al. reported an electrogram voltage reduction at the LA posterior wall not only within but also outside the encircled PVs after circumferential PVI. The authors suggested that an electrogram voltage reduction at the LA posterior wall remote from the ablated PVs, probably owing to oedematous changes, may have contributed to the modification of the arrhythmia substrate (30). The correspondence between acute oedema on MRI to regions with reduced A-EGM-biV <0.05 mV has been also shown (25).

In our study, standard catheters with relatively large distal bipole were used that record a combination of local signals and far field activity. The far-field component can be attenuated by the use of catheters with mini-electrode bipoles generating “ultra-local” tissue intracardiac electrograms. Lloyd et al. have shown, that A-EGMs characteristics from miniature embedded electrodes had greater voltages at non-ablated sites and lower voltages at ablated sites than standardly obtained A-EGMs (31). It seems that catheters with mini electrodes bring about additional benefit in distinguishing of ablated from non-ablated tissue in parallel with high spatial resolution (31). The results were

confirmed by one recent *in silico* study (32). It is plausible to hypothesize that our results (including delayed changes) could have been more prominent if A-EGMs from miniature embedded electrodes had been analyzed. However, such catheters are not established in routine AF management and our results correlate better with phenomena that may be observed in clinical practice.

The bipolar voltage might be also influenced by catheter orientation and contact force at catheter-tissue interface (33).

Despite the angulation of catheter was not exactly controlled in our study, the same transseptal sheath was used and its position was verified by fluoroscopy. We believe that individual inaccuracies were mutually nullified when high-density mapping and per-segment averaging was used. All three investigational maps were created in the same fashion, so that any systematic error was not likely involved.

It is not clear how the use of contact force sensing catheter would affect the results. Several studies did not demonstrate consistent correlation between contact force and A-EGM-biV (34–36). In our study all mapping points were manually inspected and all premature atrial beats, noisy signals and any suspected far-field EGMs were excluded from the analysis.

Limitations

Apart from above discussed points, the study has several other limitations. First, respiratory movements could also interfere with spatial accuracy of mapping points, although the respiratory variations are much less pronounced at posterior wall compared to other LA regions. Software option for respiratory compensation was disabled because this would prevent to acquire sufficient number of mapping points in limited time. Second, we cannot exclude that properties of myocardium were changed by mechanical trauma due to the repeated contact mapping. Third, the study investigated conventional RF delivery and the obtained results cannot be extrapolated to other RF ablation modes, e.g., those with high-power short-duration setting. Finally, it remains unknown whether observed changes at the posterior antrum of left PVs could be comparably reproduced in other LA regions

REFERENCES

- Kirchhof P, Benussi S, Kotecha D, Ahlsson A, Atar D, Casadei B, et al. 2016 ESC Guidelines for the management of atrial fibrillation developed in collaboration with EACTS. *Eur Heart J*. (2016) 37:2893–962. doi: 10.1093/eurheartj/ehw210
- Verma A, Kilicaslan F, Pisano E, Marrouche NF, Fanelli R, Brachmann J, et al. Response of atrial fibrillation to pulmonary vein antrum isolation is directly related to resumption and delay of pulmonary vein conduction. *Circulation* (2005) 112:627–35. doi: 10.1161/CIRCULATIONAHA.104.533190
- Morady F. Radio-frequency ablation as treatment for cardiac arrhythmias. *N Engl J Med*. (1999) 340:534–44. doi: 10.1056/NEJM199902183400707
- Khan IA. Atrial stunning: basics and clinical considerations. *Int J Cardiol*. (2003) 92:113–28. doi: 10.1016/S0167-5273(03)00107-4
- Medi C, Sparks PB, Morton JB, Kistler PM, Halloran K, Rosso R, et al. Pulmonary vein antral isolation for paroxysmal atrial fibrillation: results from long-term follow-up. *J Cardiovasc Electrophysiol*. (2011) 22:137–41. doi: 10.1111/j.1540-8167.2010.01885.x
- Datino T, Macle L, Qi XY, Maguy A, Comtois P, Chartier D, et al. Mechanisms by which adenosine restores conduction in dormant canine pulmonary veins. *Circulation* (2010) 121:963–72. doi: 10.1161/CIRCULATIONAHA.109.893107
- Lemola K, Ting M, Gupta P, Anker JN, Chugh A, Good E, et al. Effects of two different catheter ablation techniques on spectral characteristics of atrial fibrillation. *J Am Coll Cardiol*. (2006) 48:340–8. doi: 10.1016/j.jacc.2006.04.053
- Lemola K, Hall B, Cheung P, Good E, Han J, Tamirisa K, et al. Mechanisms of recurrent atrial fibrillation after pulmonary vein isolation by segmental ostial ablation. *Heart Rhythm* (2004) 1:197–202. doi: 10.1016/j.hrthm.2004.03.071
- Lo LW, Lin YJ, Tsao HM, Chang SL, Hu YF, Tsai WC, et al. Characteristics of complex fractionated electrograms in nonpulmonary vein ectopy initiating atrial fibrillation/atrial tachycardia. *J Cardiovasc Electrophysiol*. (2009) 20:1305–12. doi: 10.1111/j.1540-8167.2009.01617.x
- Haines DE, Verow AF. Observations on electrode-tissue interface temperature and effect on electrical impedance during radiofrequency ablation of ventricular myocardium. *Circulation* (1990) 82:1034–8. doi: 10.1161/01.CIR.82.3.1034
- Haines DE, Watson DD, Verow AF. Electrode radius predicts lesion radius during radiofrequency energy heating. Validation of a proposed thermodynamic model. *Circ Res*. (1990) 67:124–9. doi: 10.1161/01.RES.67.1.124

with much thicker myocardium, more complicated anatomy or presence of significant scarring.

CONCLUSIONS

Significant alteration of atrial electrograms was detectable rather distant from the center of RF ablation lesion. Spatiotemporal development of ablation lesion was eccentric/asymmetric. While acute A-EGM voltage reduction can be attributed predominantly to direct thermal injury, delayed effects are probably due to oedema progression.

ETHICS STATEMENT

This study was carried out in accordance with the recommendations of Ethics committee of the General University Hospital in Prague with written informed consent from all subjects. All subjects gave written informed consent in accordance with the Declaration of Helsinki. The protocol was approved by the Ethics committee of the General University Hospital in Prague.

AUTHOR CONTRIBUTIONS

SH participated on data collection and analysis and drafted the manuscript. HA, ZF, and LS participated on data collection and analysis. DW conceived the study design, participated on data collection and analysis, performed statistical analysis, and critically revised the manuscript for important intellectual content. All authors read and approved the final manuscript.

ACKNOWLEDGMENTS

The study was supported by Progres Q38/LF1 and by project reg. no. CZ.2.16/3.1.00/21565 from OP Prague Competitiveness. The results were partially presented as conference abstract at annual European Society of Cardiology Congress in 2017.

12. Tanno K, Kobayashi Y, Kurano K, Kikushima S, Yazawa T, Baba T, et al. Histopathology of canine hearts subjected to catheter ablation using radiofrequency energy. *Jpn Circ J.* (1994) 58:123–35. doi: 10.1253/jcj.58.123
13. Schwartzman D, Ren JF, Devine WA, Callans DJ. Cardiac swelling associated with linear radiofrequency ablation in the atrium. *J Interv Card Electrophysiol.* (2001) 5:159–66. doi: 10.1023/A:1011477408021
14. Lardo AC, McVeigh ER, Jumrussirikul P, Berger RD, Calkins H, Lima J, et al. Visualization and temporal/spatial characterization of cardiac radiofrequency ablation lesions using magnetic resonance imaging. *Circulation* (2000) 102:698–705. doi: 10.1161/01.CIR.102.6.698
15. Natale A, Newby KH, Pisano E, Leonelli F, Fanelli R, Potenza D, et al. Prospective randomized comparison of antiarrhythmic therapy versus first-line radiofrequency ablation in patients with atrial flutter. *J Am Coll Cardiol.* (2000) 35:1898–904. doi: 10.1016/S0735-1097(00)00635-5
16. Schwartzman D, Kanzaki H, Bazaz R, Gorcsan J III. Impact of catheter ablation on pulmonary vein morphology and mechanical function. *J Cardiovasc Electrophysiol.* (2004) 15:161–7. doi: 10.1046/j.1540-8167.2004.03451.x
17. Weerasooriya R, Jais P, Sanders P, Scavée C, Hsu LF, Hocini M, et al. Images in cardiovascular medicine. Early appearance of an edematous tissue reaction during left atrial linear ablation using intracardiac echo imaging. *Circulation* (2003) 108:e80. doi: 10.1161/01.CIR.00000833530.08597.B5
18. Ren JF, Callans DJ, Schwartzman D, Michele JJ, Marchlinski FE. Changes in local wall thickness correlate with pathologic lesion size following radiofrequency catheter ablation: an intracardiac echocardiographic imaging study. *Echocardiography* (2001) 18:503–7. doi: 10.1046/j.1540-8175.2001.00503.x
19. Ren JF, Callans DJ, Michele JJ, Dillon SM, Marchlinski FE. Intracardiac echocardiographic evaluation of ventricular mural swelling from radiofrequency ablation in chronic myocardial infarction: irrigated-tip versus standard catheter. *J Interv Card Electrophysiol.* (2001) 5:27–32. doi: 10.1023/A:1009849622858
20. Callans DJ, Ren JF, Schwartzman D, Gottlieb CD, Chaudhry FA, Marchlinski FE. Narrowing of the superior vena cava-right atrium junction during radiofrequency catheter ablation for inappropriate sinus tachycardia: analysis with intracardiac echocardiography. *J Am Coll Cardiol.* (1999) 33:1667–70. doi: 10.1016/S0735-1097(99)00047-9
21. Yamamoto T, Yamada T, Yoshida Y, Inden Y, Tsuboi N, Suzuki H, et al. Comparison of the change in the dimension of the pulmonary vein ostia immediately after pulmonary vein isolation for atrial fibrillation—open irrigated-tip catheters versus non-irrigated conventional 4 mm-tip catheters. *J Interv Card Electrophysiol.* (2014) 41:83–90. doi: 10.1007/s10840-014-9919-6
22. Okada T, Yamada T, Murakami Y, Yoshida N, Ninomiya Y, Shimizu T, et al. Prevalence and severity of left atrial edema detected by electron beam tomography early after pulmonary vein ablation. *J Am Coll Cardiol.* (2007) 49:1436–42. doi: 10.1016/j.jacc.2006.10.076
23. Simonetti OP, Finn JP, White RD, Laub G, Henry DA. “Black blood” T2-weighted inversion-recovery MR imaging of the heart. *Radiology* (1996) 199:49–57. doi: 10.1148/radiology.199.1.8633172
24. Yokokawa M, Tada H, Koyama K, Ino T, Naito S, Oshima S, et al. The change in the tissue characterization detected by magnetic resonance imaging after radiofrequency ablation of isthmus-dependent atrial flutter. *Int J Cardiol.* (2011) 148:30–5. doi: 10.1016/j.ijcard.2009.10.018
25. Vergara GR, Marrouche NF. Tailored management of atrial fibrillation using a LGE-MRI based model: from the clinic to the electrophysiology laboratory. *J Cardiovasc Electrophysiol.* (2011) 22:481–7. doi: 10.1111/j.1540-8167.2010.01941.x
26. Eyerly SA, Vejdani-Jahromi M, Dumont DM, Trahey GE, Wolf PD. The evolution of tissue stiffness at radiofrequency ablation sites during lesion formation and in the peri-ablation period. *J Cardiovasc Electrophysiol.* (2015) 26:1009–18. doi: 10.1111/jce.12709.
27. Wright M, Harks E, Deladi S, Fokkenrood S, Brink R, Belt H, et al. Characteristics of radiofrequency catheter ablation lesion formation in real time *in vivo* using near field ultrasound imaging. *JACC Clin Electrophysiol.* (2018) 4:1062–72. doi: 10.1016/j.jacep.2018.04.002
28. Saito T, Waki K, Becker AE. Left atrial myocardial extension onto pulmonary veins in humans: anatomic observations relevant for atrial arrhythmias. *J Cardiovasc Electrophysiol.* (2000) 11:888–94. doi: 10.1111/j.1540-8167.2000.tb00068.x
29. Udyavar AR, Huang SH, Chang SL, Lin YJ, Tai CT, Lo LW, et al. Acute effect of circumferential pulmonary vein isolation on left atrial substrate. *J Cardiovasc Electrophysiol.* (2009) 20:715–22. doi: 10.1111/j.1540-8167.2008.01411.x
30. Duytschaever MBK, Eynde GV, Tavernier R. Circumferential pulmonary vein ablation reduces electrogram voltage at the posterior wall of left atrium exterior from the encircled pulmonary veins (abstr). *Circulation* (2005) 112.
31. Lloyd MS, Hoskins MH, Shah AD, Langberg JJ. Electrogram characteristics of ablated and non-ablated myocardium in humans: a comparison of miniaturized embedded electrodes and conventional ablation electrodes. *J Cardiovasc Electrophysiol.* (2016) 27:820–4. doi: 10.1111/jce.12980
32. Pollnow S, Greiner J, Oesterlein T, Wulfers EM, Loewe A, Dossel O. Mini electrodes on ablation catheters: valuable addition or redundant information?—insights from a computational study. *Comput Math Methods Med.* (2017) 2017:1686290. doi: 10.1155/2017/1686290
33. Josephson ME, Anter E. Substrate mapping for ventricular tachycardia: assumptions and misconceptions. *JACC Clin Electrophysiol.* (2015) 1:341–52. doi: 10.1016/j.jacep.2015.09.001
34. Sasaki N, Okumura Y, Watanabe I, Sonoda K, Kogawa R, Takahashi K, et al. Relations between contact force, bipolar voltage amplitude, and mapping point distance from the left atrial surfaces of 3D ultrasound- and merged 3D CT-derived images: implication for atrial fibrillation mapping and ablation. *Heart Rhythm* (2015) 12:36–43. doi: 10.1016/j.hrthm.2014.09.007
35. Maille B, Das M, Hussein A, Shaw M, Chaturvedi V, Morgan M, et al. Accuracy of left atrial bipolar voltages obtained by ConfiDENSE multielectrode mapping in patients with persistent atrial fibrillation. *J Cardiovasc Electrophysiol.* (2018) 29:881–8. doi: 10.1111/jce.13472
36. Liang JJ, Elafros MA, Muser D, Pathak RK, Santangeli P, Supple GE, et al. Comparison of left atrial bipolar voltage and scar using multielectrode fast automated mapping versus point-by-point contact electroanatomic mapping in patients with atrial fibrillation undergoing repeat ablation. *J Cardiovasc Electrophysiol.* (2017) 28:280–8. doi: 10.1111/jce.13151

Conflict of Interest Statement: The authors declare that the research was conducted in the absence of any commercial or financial relationships that could be construed as a potential conflict of interest.

Copyright © 2019 Havranek, Alfredova, Fingrova, Souckova and Wichterle. This is an open-access article distributed under the terms of the Creative Commons Attribution License (CC BY). The use, distribution or reproduction in other forums is permitted, provided the original author(s) and the copyright owner(s) are credited and that the original publication in this journal is cited, in accordance with accepted academic practice. No use, distribution or reproduction is permitted which does not comply with these terms.